Asociación Argentina
de Mecánica Computacional

Mecánica Computacional Vol XXVIII, págs. 1283-1295 (artículo completo)
Cristian García Bauza, Pablo Lotito, Lisandro Parente, Marcelo Vénere (Eds.)
Tandil, Argentina, 3-6 Noviembre 2009

ADAPTIVE REFINEMENT OF UNSTRUCTURED FINITE ELEMENT MESHES FOR COMPRESSIBLE FLOWS

Ríos Rodriguez, Gustavo A., Storti M.A, Nigro N.M.

Centro Internacional de Métodos Computacionales en Ingeniería CIMEC
Universidad Nacional del Litoral, CONICET
Güemes 3450, 3000, Santa Fe, Argentina
e-mail gusadrr@yahoo.com.ar

Abstract. It is well known that sudden changes in the solution produced by shock waves and contact discontinuities often appear in compressible flow problems. These features of the flow field require very small size finite elements to achieve an accurate solution. However, homogeneous refinement of the whole mesh quickly becomes prohibitive for three dimensional meshes due to computational cost issues. In these situations, the use of adaptive mesh refinement strategies shows advantageous. An h-adaptive unstructured mesh refinement strategy to solve both steady and unsteady compressible flow problems by the finite element method is used in this work. The adaption algorithm is briefly introduced. The main features of the adapted meshes are the presence of hanging nodes and the controlled geometrical quality of its elements. Refinement constraints are enforced to guarantee a smooth size distribution amongst neighbour elements and a posteriori error indicators based on the gradient of the flow variables are used to track discontinuities through the flow field. The algorithm is implemented in the C++ programming language together with the STL and Boost libraries. The mesh adaption code is coupled to an SUPG-FEM flow solver which is run in parallel on a cluster of workstations. The spherical blast wave problem known as the Taylor-Sedov problem is solved with this code and the flow field is compared to that provided by the theory.

Keywords: mesh adaptivity, error indication, mesh quality, blast waves.

1 INTRODUCTION

Transonic and supersonic flow problems are common candidates for being adaptively solved by the finite element method because their most important features, namely shock waves and contact discontinuities, usually develop in a very thin region compared to the length scale of the problem domain. Adaption of the mesh allows to reduce the computational effort because of the introduction of smaller finite elements only where they are needed, thus reducing the size of the fluid dynamic problem. Here a mesh enrichment (h-adaptivity) procedure is used to achieve this goal. The meshes to be adapted are unstructured and made up tetrahedra. Hanging nodes appear in the refined meshes because no transition elements are used to match zones with different levels of refinement. Since the strategy was introduced in a series of previous works (Ríos Rodriguez et al., 2005, 2006, 2008) and was also described in detail in Ríos Rodriguez (2009), only its main features are highlighted. The developed algorithm and the C++ code derived from it have already been used to solve 2-D, 3-D and axisymmetric inviscid compressible flow problems.

The mesh adaptation is sequentially performed on a single processor of a Beowulf cluster (not necessarily the server node) while the solution of the fluid dynamic problem is computed in parallel. The three dimensional Euler equations are solved with the advection-diffusion module of the PETSc-FEM code (Storti et al., 1999-2008). This solver implements both the SUPG formulation introduced by Brooks and Hughes (1980, 1982) to stabilize the advection term and shock capturing techniques for the treatment of strong shocks. Both the adaption of the mesh and the solution of the equations are coupled through a driver module which performs suitable calls to the adaption function or to the equations solver.

The spherical blast wave problem as described by Taylor (1946, 1950a,b) and Sedov (1959) is solved. The adapted solution is compared to a similar one computed with a fixed mesh and to that obtained by solving a set of ordinary differential equations which are derived from the Euler equations by following the Taylor-Sedov assumptions. Conclusions are drawn from the FEM solution accuracy and the computational costs.

2 ADAPTION STRATEGY

The following are the main features of the adaption strategy:

1. To keep bounded the geometrical quality decrease of the mesh is the main driving force in the design of the refinement strategy. In this sense, only 1:4 and 1:8 regular refinement patterns are applied for 2-D and 3-D respectively and no transition elements are used. However since no regular 1:8 subdivision exists for tetrahedra a refinement scheme that shows a good between the computational effort and the geometrical quality of the *child* elements is chosen. In Ríos Rodriguez (2009) it is shown through numerical experiments that refining the *parent* tetrahedron by joining the midpoints $(a_0, \ldots, a_5)$ of the edges with new ones and choosing then the shortest diagonal of the inner octahedron (see sequence a)-b)-c) in figure 2) to get the four remaining tetrahedra is a good refinement strategy. In those experiments, the geometrical quality of the tetrahedra was measured with both geometric and algebraic quality metrics such as the dihedral angles and the mean ratio shape measure introduced by Liu and Joe (1994).

2. Starting from a conforming unstructured finite element *base* mesh, a succession of nested nonconforming meshes is generated. It is worth to mention that although the adapted meshes introduce hanging nodes on the edges or faces of an element, constraining the

solution at these nodes ensures continuity of the numerical solution amongst nearby elements through that edge or face. That is, the flow field variables on hanging nodes are computed as the average of the flow variables for the nodes that define the edges or faces (hexaedron) to which these hanging nodes belongs (see figure 1).

3. Coarsening of the base mesh is not allowed.

4. Refinement rules or constraints are applied to ensure uniform element size distribution.

5. Multiple refinement / derefinement levels are allow each time the mesh is updated.

6. Boundary conditions and other properties of the mesh entities are handled by a property identifier associated to the entities of the base mesh. This property identifier is inherited from a parent geometrical entity of the mesh to its child during the adaption procedure. The identifier is defined by the user beforehand and it can describe a set of features of different "nature" for that entity. For example: the identifier assigned to a face could mean that a slip boundary condition has to be enforced on that face and also that the face belongs to a curved surface which defines a particular section of the boundary.

7. The state of the flow variables computed for the last adapted mesh is projected on the new mesh to restart flow calculation.

8. Adaption of the mesh is only allowed after the solution has been advanced a fixed number of time steps. That is, the updating frequency of the mesh being used to solve the fluid dynamic problem is constant throughout the whole simulation. However the time step size is updated with the same frequency to satisfy the Courant-Friedrich-Lewy (CFL) condition. In practice it is found that the adaption of the mesh and the boundary conditions plus the projection of the state takes a small fraction of the total computation time ($\lesssim 5$ per cent) for unsteady three dimensional problems. This leads to choose a high updating frequency for the mesh (~5 time steps) for not compromising the overall performance of the adaptive solution procedure. If the time required by the adaption of the mesh were found to be a greater percentage of the overall computing one then a lower updating frequency should be chosen. In this case, however, a bigger cost would be transferred to the flow computation stage since the refined regions of the mesh would need to be wider to ensure the discontinuities are kept inside these regions until the mesh is updated again. Choosing a high frequency for adapting the mesh enables to use narrower refined regions around discontinuities and to further reduce the size of the fluid flow problem.

9. Selection of the regions of the mesh that need to be refined is accomplished by means of error estimation. For compressible flow problems the gradient of the density or pressure are commonly used with acceptable results. Gradient reconstruction techniques based on the Zienkiewicz and Zhu (1987) formulation are also implemented in the code. Reconstruction of the gradient field at a vertex of the mesh is achieved by a weighted averaging of the gradient on the patch comprised by all the elements that surround that vertex.

Items 4 and 7 are further explained in the following subsections.

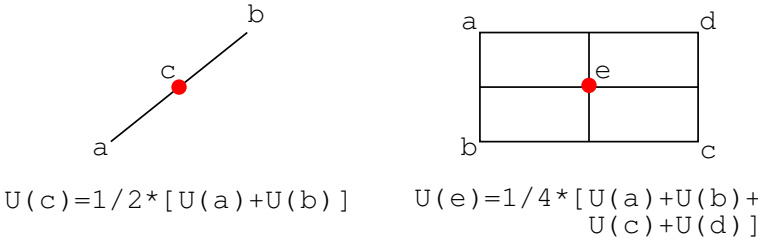

Figure 1: Solution constraint for a hanging node over an edge or quadrilateral face.

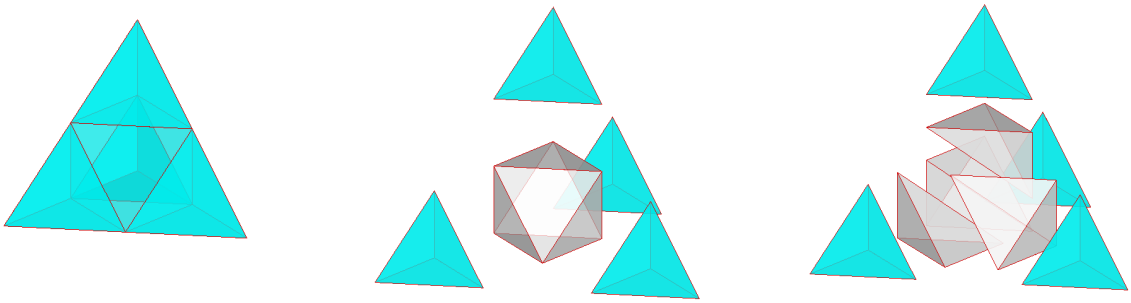

(a) (b) (c)

Figure 2: Tetrahedron refinement sequence.

2.1 Refinement constraints

Besides high geometrical quality elements, a smooth transition in the size of the elements is also desired since the condition number of the global stiffness matrix in the finite element method also depends on the size distribution of the mesh elements (Schewchuck, 2002). To this end, a refinement rule was introduced by Babuska and Rheinboldt (1978) for 2-D meshes. This rule says that *no more than one hanging node should be shared amongst nearby elements through the common edge to which the hanging node belongs*. Figures 3.a) and 3.b) shows that applying this constraint guarantees that neighbour elements introduced by the refinement of the mesh will not have very different sizes (irregular nodes are marked as red dots). To this end, the neighbour element that shares the parent *active*[1] edge of the edge which belongs to the element selected to be refined has also to be refined. However, this constraint does not take into account special situations that appear for 3-D meshes, as it is shown in figure 4 for tetrahedral elements.

(a) (b)

Figure 3: Refinement constraint for 2-D meshes.

[1]It is said that an edge or face is active as long as not all the elements that are neighbour through it are refined.

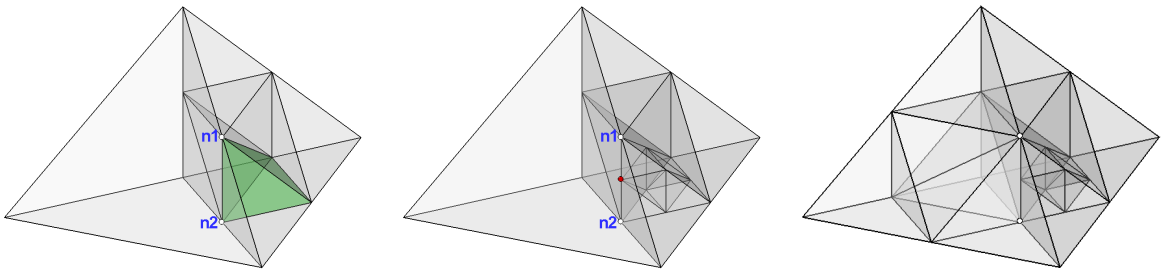

(a) (b) (c)

Figure 4: Refinement constraint for 3-D meshes - Orphan edge case.

In three dimensions, the neighbourhood through edges and faces as well as the refinement of *orphan* edges[2] over shared faces have to be taken into account. In figure 4.a) the green-colored element is selected to be refined. As a consequence an orphan edge (i.e.: the edge defined by the nodes $n1$ and $n2$) on the shared face needs to be refined. It is seen in figure 4.b) that if the two dimensional constraint were only applied this situation would be allowed. But then a difference of more than one level of refinement would exists amongst nearby elements in the mesh. Figure 4.c) shows that adding the element that shares the face such that at least one of its orphan edges has been refined copes with the problem.

2.2 State projection

A new state on the new adapted mesh has to be supplied as an initial condition to restart the flow computation. When the base mesh is adapted for the first time, linear interpolation of the flow variables is used to assign the state to the newly created vertices of the refined mesh. This is enough in order to guarantee conservation of the flow variables if a linear finite element formulation is used and if the new points are placed in the middle of the edges, or barycenter of faces or elements.

After the mesh and its corresponding boundary conditions are adapted and an interpolated state is supplied, the flow calculation is resumed for a fixed number of time steps. The solution is advanced in time and a new state is computed. Then the error estimator is applied and the mesh is updated again. For all the adaption steps except for the first one, the state is projected as follows: given a vertex V in the recently updated mesh (adaption step n) it is required to find the element in the previously adapted mesh (adaption step $n-1$) that contains it. This is done through an approximate nearest neighbour search using the ANN library (Arya and Mount, 2006). The barycenter of the elements that belong to the $(n-1)$ adaption step are computed to this end. This approximate search provides a list of k-nearest elements $l_V = \{e_1, e_2, \ldots, e_k\}$ to vertex V. These elements are candidates for containing V and the value of k is chosen beforehand. Then, it is possible to find the element that contains vertex V by computing the volume or area coordinates $N_j^{(e_i)}$, $j = 1, \ldots, ne$ for each one of the candidates at this vertex. Here ne is the number of nodes per element and j is the index of the local vertex in the element. If any of the volume coordinates $N_j^{(e_i)}$ is less than zero, point V is outside of element e_i and the next element in l_V is checked. Only if all the volume coordinates for that element are greater

[2]Edges that are not obtained by the refinement of another edge are said to be *orphans* or with no parents.

than or equal to zero it can be stated that V is inside element e_i or over one of its faces or edges. In this case traversal of l_V is interrupted and the state vector is computed as follows

$$\mathbf{U}_V^{(n)} = \sum_{j=1}^{Ne} N_j^{(e_i)}(\mathbf{x}_V) \cdot \mathbf{U}_j^{(n-1)} \tag{1}$$

where $\mathbf{U}_j^{(n-1)}$ is the state vector defined at local vertex j of the element e_i at adaption step $n-1$, $\mathbf{x}_V$ is the coordinate vector of vertex V and $\mathbf{U}_V^{(n)}$ is the state vector for vertex V at adaption step n. Dashed lines in figure 5.a) illustrate the volume coordinates at vertex V while figure 5.b) shows the situation for the current adaption step.

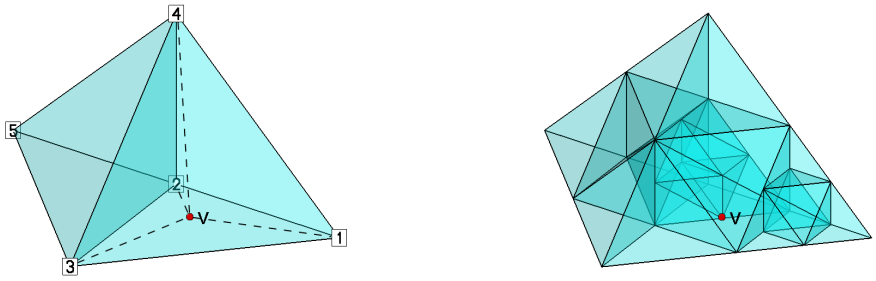

(a) Vertex position at adaption step n-1

(b) Vertex position at adaption step n

Figure 5: State projection - Finding vertex position

3 TAYLOR-SEDOV SELF-SIMILAR SOLUTION FOR THE SPHERICAL BLAST WAVE PROBLEM

The blast wave problem, also known as the Taylor-Sedov problem, describes what happens if a point-like explosion occurs in a uniform density gas. After a short lapse of time one expects to find a spherical shock wave traveling radially outward at supersonic speeds with a subsonic flow behind it. This shock wave comes to an end because the source of pressure (.i.e. the release of energy) also comes to an end. This allows the rarefaction wave generated in the center of the explosion to weaken the spherical shock until it becomes a pressure wave. When this kind of phenomena takes place it is said that a blast wave happens.

Taylor and Sedov analysis assumes a self-similar solution for the blast wave problem, which means that the solution profiles for the density ρ, velocity u and pressure p keep their shape in time and depend only on a single parameter ξ that is defined as the ratio between the radial coordinate r measured from the center of the explosion and the spherical shock wave position R. Taylor and Sedov formulate the following relationship between the physical variables and the self-similar profiles for the velocity $U(\xi)$, density $\Omega(\xi)$ and pressure $P(\xi)$

$$u = \dot{R}U(\xi), \quad \rho = \rho_0\Omega(\xi), \quad p = \rho_0\dot{R}^2P(\xi) \tag{2}$$

This solution holds as long as the mass swept up by the spherical shock front is much greater than the mass of the explosive material and as long as the shock wave can be considered strong (see Thorne (2002)). The equations for the self-similar solutions are derived from the Euler

equations in radial coordinates. The latter can be reduced to a system of ordinary differential equations if it is further assumed that the density shows a power law dependence in space and time and if the shock front position obeys to a power law in time. Then the ODE's are numerically integrated with a forth order Runge-Kutta method assuming the following boundary conditions immediately behind the shock front (at $\xi = 1$)

$$U = \frac{2}{\gamma+1}, \quad \Omega = \frac{\gamma+1}{\gamma-1}, \quad P = \frac{2}{\gamma+1} \tag{3}$$

The self-similar computed profiles plotted against the similarity parameter are shown in figure 6. It is seen that the pressure in the center of the blast wave is almost half the maximum pressure immediately behind the shock and it is fairly uniform within the blast wave. It can also be seen that most of the ambient gas mass processed by the shock wave is compressed within a thin spherical shell immediately behind the shock which moves slightly slower than the shock itself ($u \simeq 0.83\dot{R}$ if $\gamma = 1.4$). Finally the velocity profile is almost linear in the blast wave, with the fluid being at rest in the center of the explosion.

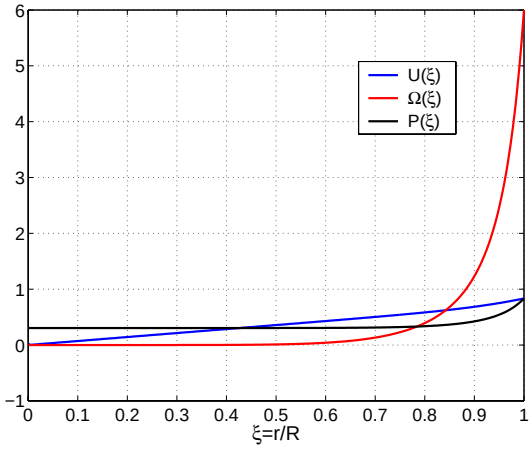

Figure 6: Self-similar profiles for the spherical blast wave problem ($\gamma = 1.4$).

By a simple dimensional analysis it can be found that

$$R(t) \propto \left(\frac{E_x}{\rho_0}\right)^{1/5} t^{2/5} \tag{4}$$

where E_x is the energy released by the explosive material. The constant of proportionality Q that allows to equate both sides of eq.(4) can be computed by numerical integration of the total energy profile for a given time instant

$$E_x = \int_0^R \left(\frac{p}{\gamma-1} + \frac{\rho u^2}{2}\right) 4\pi r^2 dr \tag{5}$$

Changing to variable ξ and substituting u, p and ρ from eqs.(2) in the integral of eq.(5), taking into account that $\dot{R} = \frac{2}{5}\frac{R}{t}$, then replacing E_x given by eq.(5) into eq.(4) and finally solving for Q it is found

$$Q = \left(\frac{16\pi}{25} \int_0^1 \left(\frac{P(\xi)}{\gamma - 1} + \frac{\Omega(\xi) U(\xi)^2}{2} \right) \xi^2 d\xi \right)^{-1/5} \tag{6}$$

4 FINITE ELEMENT SOLUTION

The numerical problem is solved on a spherical domain of radius $R_{ext} = 5$m. The following initial conditions are assumed: the ambient gas (air) is at rest and the pressure and density are constants equal to $p_0 = 101325$Pa and $\rho_0 = 1.225$kg/m^3 respectively. It is assumed that the energy released by the explosive instantly raises the pressure to $p_{blast} = 10^5 \cdot p_0$ in a small spherical region of radius $R_{blast} \simeq 0.25$m. The initial explosion is not simulated in this work but it is considered to be a constant volume thermodynamic evolution. The pressure fixation at the surface of the spherical domain is the only boundary condition prescribed. This condition is adequate as long as the shock wave does not reach this boundary.

Tetrahedral elements are used to subdivide the problem domain. Finite elements of smaller size are prescribed towards the center of the sphere. The resulting mesh has 421.000 tetrahedra and 76.500 vertices approximately. This mesh is used for both simulations, namely as the base mesh for the adaptive simulation and as the only mesh for the non-adaptive one.

The Euler equations are solved in parallel with 15 processors of a cluster of workstations and a Backward-Euler scheme is used for time integration. The magnitude of the density gradient is chosen as the error indicator for the adaptive simulation since the flow field generated by the blast wave is dominated by a strong shock and an expansion wave,

$$c_1 \leq \frac{\| \nabla_i \rho \| \cdot h_i}{\max_i (\| \nabla_i \rho \| \cdot h_i)} \tag{7}$$

c_1 is a constant set beforehand by the user of the adaption code, h_i is a measure for the size of the element and $\| \nabla_i \rho \|$ is the magnitude of the density gradient computed for that element. A $c_1 \simeq 0.15$ value is used in the simulations. An updating frequency of 10 time steps is chosen and a maximum of 2 levels of refinement is prescribed. The final time for both simulations is equal to $t_f \simeq 0.001$s.

4.1 Numerical results

In comparing the position of the shock front to that given by eq.(4) it is taken into account that the FEM solution profiles will approximate the shape of the theoretical ones just after a few time steps, since the initial condition for the flow variables does not conform to the self-similar profiles of the theory. Bearing this in mind, figure (7) shows the shock wave position as a function of time for both the simulations and the analytical solution given by eq.(4). It can be stated that although there is a good agreement for the first time instants, the adaptive and non-adaptive simulations lug behind the analytical one by almost 15% and 13% respectively at $t = 0.00045$s. The analytical solution is computed with a value $Q \simeq 1.1653$ for the constant in eq.(6) as given by Hutchens (2000).

The solution profiles along the radius behave like those given by the self-similar theoretical solution. Figure 8.a) shows that the pressure within the blast wave is fairly uniform and has a value that is half the maximum reached immediately behind the shock (notice that the pressure axis is in logarithmic scale). The Mach number within the blast wave is depicted in figure 8.b). It can be seen that it is fairly subsonic in the whole domain, as it is expected for the flow produced by a supersonic unsteady strong shock wave traveling through a gas at rest (actually,

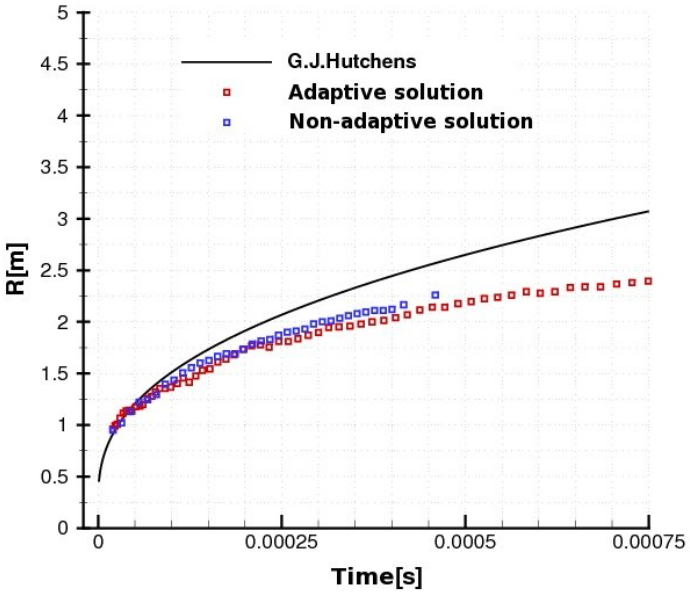

Figure 7: Shock wave position as a function of time.

the shock wave travels roughly at an average speed of 3000m/s for the simulated final time t_f). The density profiles in figure 8.c) show, as well as the other variables, that the entire flow field is better resolved for the adaptive solution because no spurious oscillations appear in the expansion region behind the shock wave and the latter is sharply defined. Finally, figure 9.a) depicts a cut of the mesh on a plane of symmetry at $t = 0.645$ms while figure 9.b) shows the corresponding pressure field and isolines. The mesh has ~2.34 million tetrahedra and 4.28e+5 vertices.

4.2 Mesh adaption cost

Clock time for the adaption of the mesh and the equations solution is measured for the simulation. The adaption time t_{adapt} is defined as that required to realize all the necessary tasks to adapt the mesh, namely the error indication computation, the refinement of the elements, the boundary conditions update, the state projection, the time step size computation and the writing to disk of all the files required by the solver. On the other hand, the solution time t_{sol} takes into account both the time required to advance the solution and the overhead incurred to restart the flow computation. Overall time is then defined as $t_{all} = t_{adapt} + t_{sol}$. Figure 10 shows that the ratio t_{adapt}/t_{all} keeps almost constant and equal to 0.04, which enables to state that, for this particular problem, the adaption of the mesh takes just a small fraction of the solution time. The overall time of the simulation is 71 hours and 16 minutes. Given that the biggest effort is involved in the solution of the flow equations, maybe a higher updating frequency for the mesh could have been used.

5 CONCLUSIONS

The mesh adaption strategy introduced in Ríos Rodriguez (2009) was used to solve the spherical blast wave problem, improving the sharpness of the shock front and removing the spurious oscillations in the expansion which are present in the non-adapted mesh solution. The behaviour

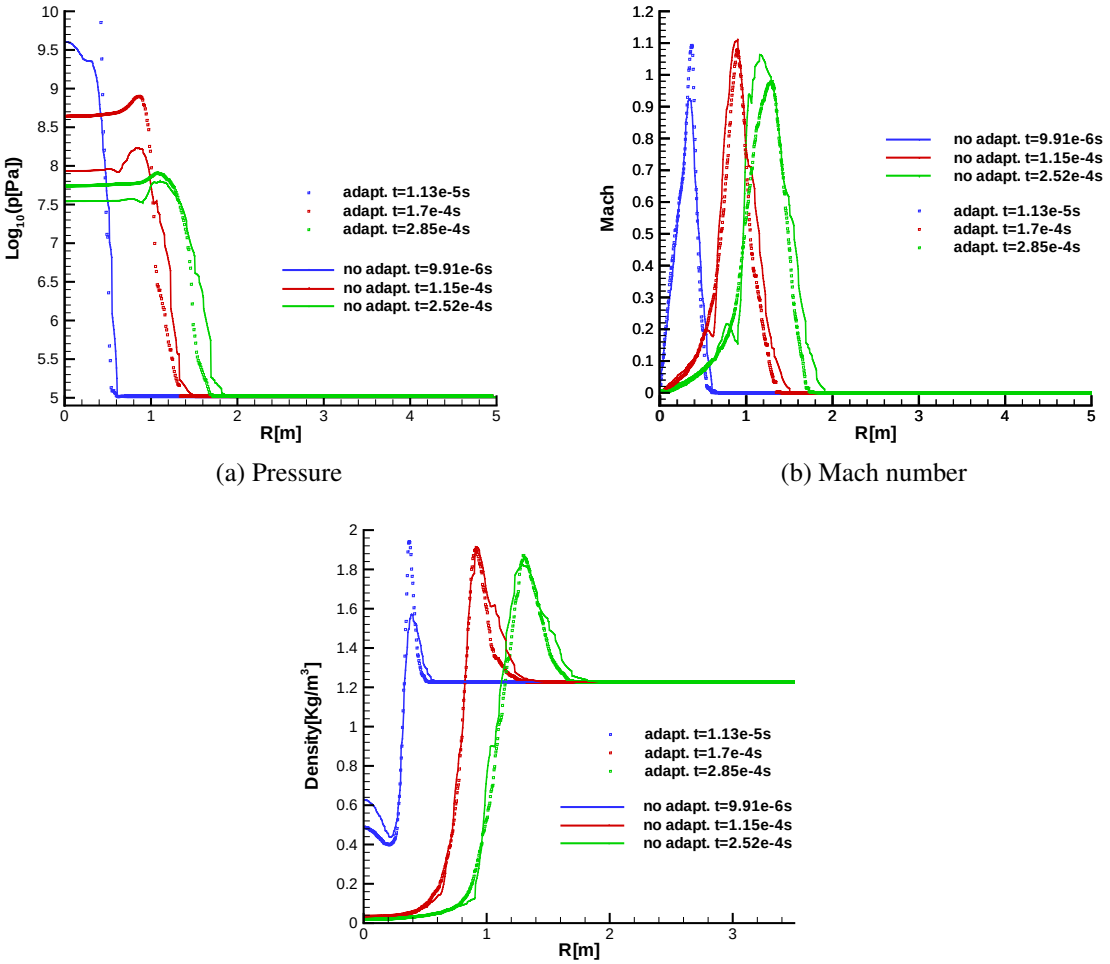

(a) Pressure

(b) Mach number

(c) Density

Figure 8: Adapted vs. non-adapted solution profiles.

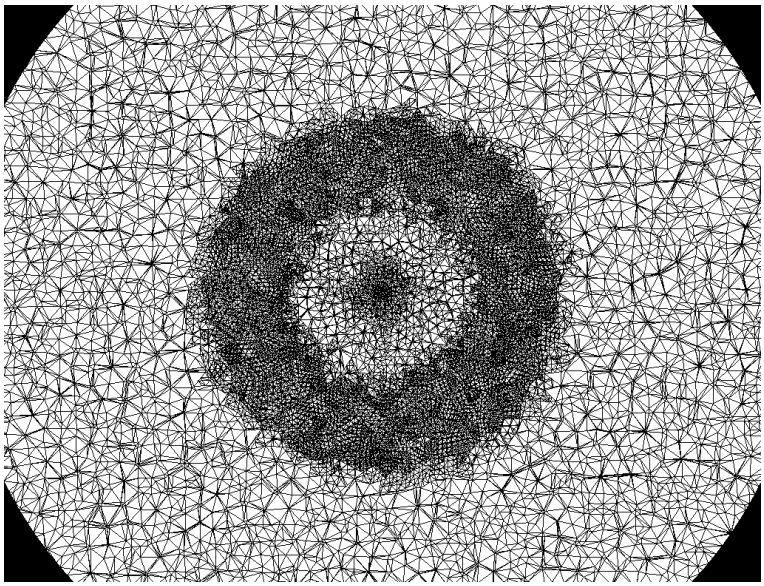

(a) Mesh cut

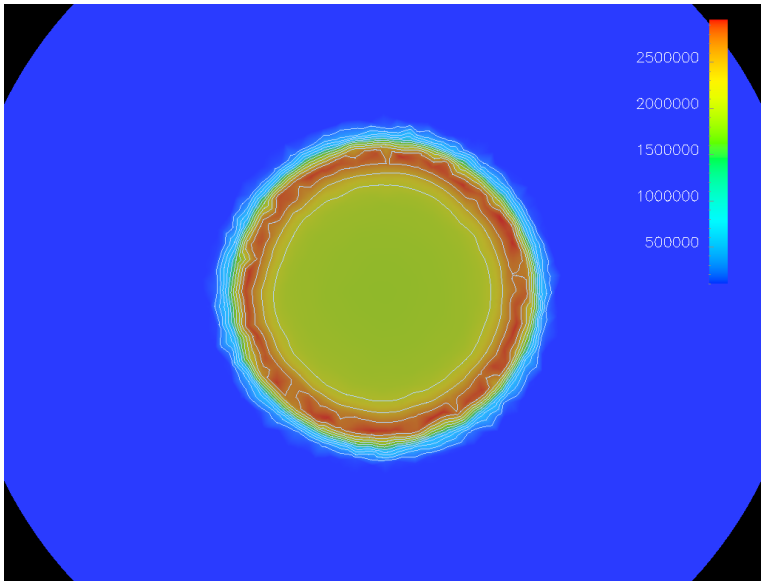

(b) Pressure field and isolines

Figure 9: Adapted mesh and pressure field on a plane of symmetry at time $t = 0.645$ms.

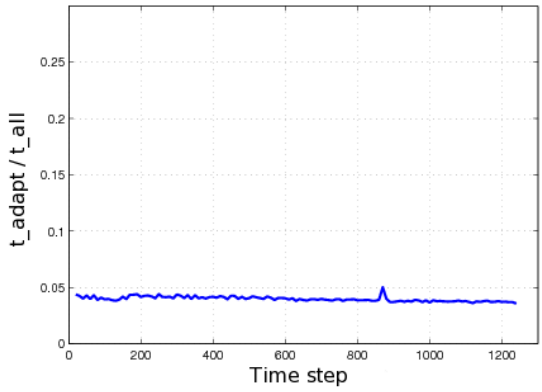

Figure 10: Relative cost for the mesh adaption at the 3-D Taylor-Sedov problem.

of the flow field variables agrees rather well with the theoretical results from the Taylor and Sedov self-similar solution. Although the shock wave position is not accurately predicted this cannot be ascribed to the adaption of the mesh since the non-adapted solution also shows a similar lack of precision. It is thought that this is due to the lack of precision of the time integration scheme used to solve the flow equations.

The overhead introduced by the adaption of the mesh is just a small percentage of the time required to compute the flow, thus allowing to greatly reduce the computational effort. If we were to solve the problem with a fixed mesh and a similar precision (in fact, if each tetrahedron of the base mesh used for the simulations and then their corresponding sons were refined following the 1:8 pattern used by the adaption procedure), a fixed mesh made up of 26.9 million would have been required!!!. So it is concluded that true benefits are achieved because of adapting the mesh, namely an accuracy improving and a reduction in the computational effort.

Acknowledgment

This work has received financial support from Consejo Nacional de Investigaciones Científicas y Técnicas (CONICET, Argentina, grant PIP 5271/05), Universidad Nacional del Litoral (UNL, Argentina, grant CAI+D 2005-10-64) and Agencia Nacional de Promoción Científica y Tecnológica (ANPCyT, Argentina, grants PICT-01141/2007). Authors made extensive use of freely distributed software as GNU/Linux OS, MPI, PETSc, GCC compilers, Octave, Open-DX, Boost, LyX, Python, Perl, VTK, amongst many others. ————————-

REFERENCES

Arya S. and Mount D. *ANN: Approximate Nearest Neighbors Library*. Department of Computer Science, University of Maryland, 2006.

Babuska I. and Rheinboldt W. Error estimates for adaptive finite element computations. *SIAM J.Numer.Anal*, 15:736–754, 1978.

Brooks A. and Hughes T. Streamline Upwind/Petrov Galerkin methods for advection dominated flows. In *Third Internat. Conf. of Finite Element Methods in Fluid Flow*. Banff, Canada, 1980.

Brooks A. and Hughes T. Streamline Upwind/Petrov Galerkin formulations for convective dominated flows with particular emphasis on the imcompressible Navier-Stokes equations. *Comput. Mehods Appl. Mech. Engrg.*, 32:199–259, 1982.

Hutchens G. Approximate near-field blast theory: A generalized approach. *Journal of Applied Physics*, 88(6):3654–3658, 2000.

Liu A. and Joe B. On the shape of tetrahedra from bisection. *Mathematics of Computation*, 63(207):141–154, 1994.

Ríos Rodriguez G. *Refinamiento H-Adaptativo de Mallas No Estructuradas en Problemas Estacionarios y Transitorios de Flujos Compresibles.* Ph.D. thesis, Universidad Nacional del Litoral, Argentina, 2009.

Ríos Rodriguez G., López E., Nigro N., and Storti M. Refinamiento adaptativo homogéneo de mallas aplicable a problemas bi- y tridimensionales. 2005.

Ríos Rodriguez G., Storti M., and Nigro N. Refinamiento adaptativo en problemas no estacionarios. 2006.

Ríos Rodriguez G., Storti M., and Nigro N. An h-adaptive unstructured mesh refinement strategy for unsteady problems. *Latin American Applied Research*, 2008. Article in press.

Schewchuck J.R. What is a good linear finite element? interpolation, conditioning, anisotropy and quality measures, 2002. URL http://www.cs.berkeley.edu/ jrs/papers/elemj.ps.

Sedov L. *Similarity and Dimensional Methods in Mechanics*. Academic Press, New York, 1959.

Storti M., Nigro N., Paz R., Dalcin L., Battaglia L., Lopez E., and Ríos Rodriguez G. *PETSc-FEM, A General Purpose, Parallel, Multi-Physics FEM Program*. CIMEC-CONICET-UNL, 1999-2008.

Taylor G. The air wave surrounding an expanding sphere. In *Mathematical and Physical Sciences*, volume 186 of *Series A*, pages 273–292. Royal Society of London, Royal Society, 1946.

Taylor G. The Formation of a Blast Wave by a Very Intense Explosion. I. Theoretical Discussion. In *Mathematical and Physical Sciences*, volume 201 of *Series A*, pages 159–174. Royal Society of London, Royal Society, 1950a.

Taylor G. The Formation of a Blast Wave by a Very Intense Explosion. II. The Atomic Explosion of 1945. In *Mathematical and Physical Sciences*, volume 201 of *Series A*, pages 175–186. Royal Society of London, Royal Society, 1950b.

Thorne K. Applications of classical physics. 2002. Www.pma.caltech.edu/Courses/ph136/yr2002.

Zienkiewicz O. and Zhu J. A simple error estimator and adaptive procedure for practical engineering analysis. *Int. J. Numer. Meth. Engineering*, 24:337–357, 1987.